# Hydrodynamically synchronized states in active colloidal arrays

**Loïc Damet,**[a] **Giovanni M. Cicuta,**[b] **Jurij Kotar,**[a] **Marco Cosentino Lagomarsino,**[c] **and Pietro Cicuta**[*a]

Colloidal particles moving in a low Reynolds number fluid interact via the induced velocity field, described to a good approximation by the Oseen tensor. We consider the collective dynamic states for a class of actively forced colloids, driven by harmonic potentials via a non-linear switching rule that couples forces to configurations, establishing oscillations between prescribed positions. Experiment, simulations and theoretical arguments show that these states are determined by the equilibrium eigenmode structure of the Oseen interaction matrix and thus by the system's geometry. The stable dynamical state is predominantly formed by the eigenmode with longest relaxation time. This has the surprising consequence that while 2 particles, or polygonal arrays of 4 or more colloids, synchronize with the nearest neighbors in anti-phase, 3 equally spaced colloids synchronize in-phase. Odd-numbered arrangements with 5 or more particles sustain traveling waves. The emerging complex dynamical state can therefore be predicted from the simple mean spatial configuration of the active colloids, or equivalently from an analysis of their fluctuations near equilibrium.

## 1 Introduction

At low Reynolds number, when inertia is irrelevant, the motion of a fluid is described by Stokes' equation, whose fundamental solution, the Oseen tensor, $H(\mathbf{r}) = (I + \hat{\mathbf{r}}\hat{\mathbf{r}})/8\pi\eta r$ (where $I$ is the identity 3x3 matrix and $\eta$ is the fluid viscosity) dictates the velocity field of point-like objects applying a force on the fluid, which decays as the inverse distance $r$. Hence the Oseen tensor describes a long-range, and often dominating, interaction in flowing colloidal systems. Force transduction through the velocity field has key consequences in diverse biological phenomena such as the motility of microorganisms[1], circulation in the brain[2] and functioning of the ear[3]. In various tissues, a macroscopic number of cilia display synchronized dynamics, or so-called "metachronal waves"[4]. Nearby cilia may beat in-phase or out of phase, and may be in a condition where is it possible to readily switch between the two dynamical states[1].

One outstanding question is what determines the character of the dynamical steady state. Recent progress in "hydrodynamic synchronization" is reviewed in ref[5]; see ref[6] for an overview of low Reynolds number (Re) flows. Despite the complexity of the biological cilia structure, and its driving mechanisms, it is possible to study the issue of synchroniza-

tion on much simpler systems, because in the far field limit the hydrodynamic flows (and hence interaction) do not depend on the detailed configuration of the driving object. Indeed the beating filament can be "replaced" by a solid sphere, driven in periodic fashion. In an attempt to model (both experimentally and theoretically) the physics of hydrodynamic synchronization, two main ideas have emerged. The first is to consider the coupling of two or more objects driven by a constant force over closed two-dimensional differentiable orbits[7]. Within this cilia model, the phase of each "rotor" is free, and there can be synchronization of different rotors under certain conditions, recently studied very generally in ref[8]. A different, one-dimensional model consists of a "geometric switch", and was proposed in ref[9]; here the force is discontinuous, and this is not described within the formalism of ref[8]. We previously investigated the geometric switch model for the simple case of two active elements, showing the robustness of synchronization in the presence of noise[10]. A linear chain of geometric-switch oscillators was studied numerically, in the absence of noise[11], and shown to have different synchronized states depending on the structure of the internal drive. However, no simple recipe is available to predict the synchronized state.

In this work we show by experiment and simulations how the non-equilibrium dynamical behavior of the geometric switch model can be understood from the eigenmode structure of the Oseen interaction tensor, and thus on the system geometry, without the need of solving complicated dynamic equations. We consider systems of a small number of elements in the presence of thermal noise: between three and five colloidal

*[a] Cavendish Laboratory and Nanoscience Centre, University of Cambridge, CB3 0HE, U.K.. E-mail: pc245@cam.ac.uk*
*[b] Dip. Fisica, Università di Parma, and INFN, Sez. Milano-Bicocca, gruppo di Parma, Italy*
*[b] Genomic Physics Group, UMR7238 CNRS "Microorganism Genomics", University Pierre et Marie Curie, 15, rue de l'École de Médecine Paris, France*
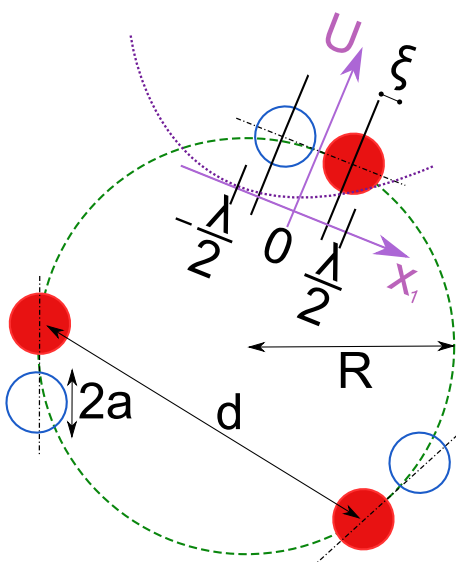
**Fig. 1 Sketch of experimental configuration.** Colloidal spheres are trapped by a harmonic potential realised by an optical trap. For each bean, the trap is centered at one of two positions: $-\lambda/2$ or $+\lambda/2$. The choice of potential is dictated by the particle position; the potential is switched when the bead arrives within $\xi$ of the active trap. Experiments and simulations are carried out varying the number of particles $N$ from $N = 3$ to $N = 5$ (and beyond, numerically); the circle radius $R$ is increased to maintain constant the distance between bead centers $d = 2R\sin(\pi/N) = 8\,\mu$m. The optical tweezers system performs image analysis on every frame to determine particle positions, and thus implement the "geometric switch" condition described in the text, at rates between 200 and 300 frames/s. Each colloidal particle in the system is effectively a phase oscillator, undergoing a motion bound in amplitude but free in period and phase. The oscillators are driven independently, and coupled only by the flow field in the liquid.

particles are arranged on equally spaced average positions on a circumference (larger systems are studied numerically), and each one is driven in small tangential oscillations, with fixed amplitude but free phase and period. The main result is that the fundamental (longest lived) hydrodynamic mode (an easily derivable quantity, in contrast to finding full solutions of the system) dominates the collective motion in the driven steady state. As a consequence, the steady state can be strikingly different depending on the number of particles and their arrangement.

This system is realized experimentally with optical traps, with fast video feedback to impose the fixed amplitude driven oscillation. The only interaction between the elements is through the hydrodynamic flow arising from the colloid movements. As a further consequence of hydrodynamic interaction, there are correlations in the Brownian fluctuations of different

particles. The dynamics of systems where spheres are held by fixed harmonic potentials on the vertices of arbitrary planar regular polygons has been solved exactly within Oseen's description of hydrodynamics [12], giving a basis from which to understand the active scenario.

## 2 Materials and Methods

### 2.1 Experimental System

Optical traps are used to confine colloidal beads within harmonic potentials, the system hardware is described in greater detail in refs [10,13]. In this work, a varying number of silica beads of radius $a = 1.5\,\mu$m (Bangslabs) are trapped from below by a time-shared laser beam, focussed by a water immersion objective (Zeiss, Achroplan IR 63x/0.90 W). A pair of acousto-optical deflectors (AOD) allows the positioning of the laser beam focus anywhere in one plane, with sub-nanometer precision; time-sharing is at a rate $\sim 10^5$ Hz, corresponding to negligible diffusion of the beads in each laser cycle. The solvent is a solution of glycerol (Fisher, Analysis Grade) in water (Ultrapure grade, ELGA) 50% w/w, giving a nominal viscosity of $\eta = 6$ mPa s at $20^o$C [14]. Experiments are performed in a temperature controlled laboratory, $T = 21^o$C. The trapping plane is positioned $(20 \pm 1)\,\mu$m above the flat bottom of the sample, in a sample volume that is around $100\,\mu$m thick.

To realize the geometric switch condition, an active driving of each colloid is implemented here, similarly to [10], but for 3, 4 or 5 particles, driving the colloids on segments tangential to the ring on which they are positioned on average, see Figure 1. A boundary is set at a pre-defined particle position, a distance $\xi$ from the minimum of the currently active optical trap. The trapped particle moves (on average) towards the trap minimum and, when it crosses the boundary, the current trap is switched off and the other trap, with its minimum a distance $\lambda$ away, is activated; the amplitude of oscillations is $\lambda - 2\xi$. In the experiments this process is implemented via image analysis in the computer giving particle positions on each camera frame, and feedback is sent to the AOD for laser deflection (and as a condition in the numerical simulations). Since the configuration is analysed experimentally only at each frame, the corresponding time interval should be considered as a feedback time (see brief discussion in Appendix). Colloidal particles are always being driven, never reaching the minimum of the active trap.

The optical trap potential is harmonic to a very good approximation, with stiffness $\kappa$ in the range 1.0 to 2.6 pN/$\mu$m, depending on the number of beads trapped (before each run, $\kappa$ is calibrated from the distribution of displacements in static traps, with precision $\pm 0.2$ pN/$\mu$m). The relaxation time $\tau_0 = \gamma/\kappa$ (where $\gamma$ is the Stokesian drag $\gamma = 6\pi\eta a$) is of the order of 0.1s. The experiments have been performed with $\lambda = 2\,\mu$m, $\xi = 0.31\,\mu$m and $d = 8\,\mu$m. The period of an isolated oscillator
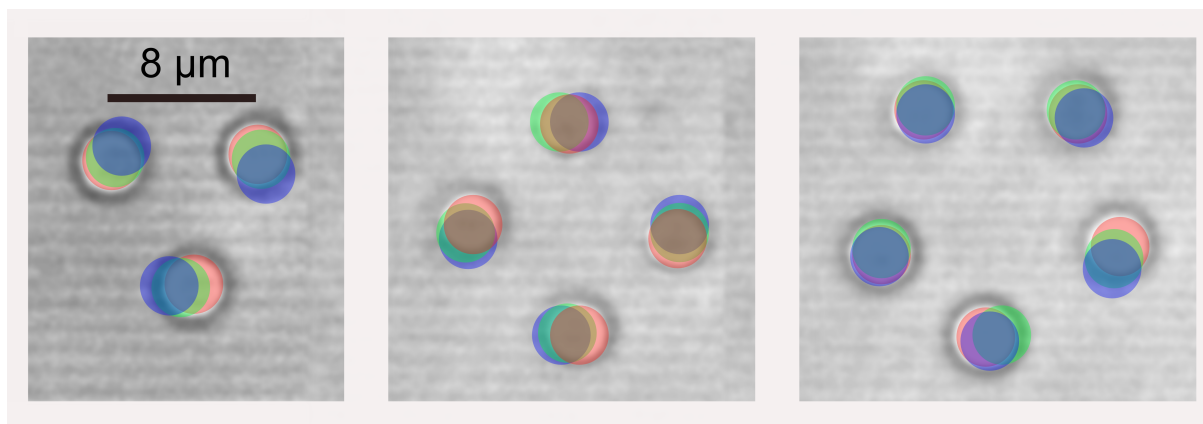
**Fig. 2 Regular arrays of actively driven colloidal particles synchronize into steady collective dynamical states.** Images showing one snapshot of the system, where the particles are highlighted in red. Particle positions after 20 frames (green) and 40 frames (blue) are overlayed. Videos are available as SM, and show clearly the $N = 3$ system performing in-phase oscillations, the $N = 4$ with neighbors in anti-phase, and $N = 5$ with phase locking between neighbors.

is $T_0 = 2\tau_0 \log[(\lambda - \xi)/\xi]$ (in the absence of noise)[10], which under the experimental conditions is about 0.3 s. With image acquisition through an AVT Marlin F-131B CMOS camera, operating at shutter aperture time of 1.5 ms, and frame rate between 200 and 300 fps (depending on the ring size, hence captured region of interest) there are multiple frames captured within the relevant timescales $\tau_0, T_0$. Video is acquired for over 4 minutes, i.e. over 48000 frames. There is typically a transient lasting around a few periods before the systems reach the steady state discussed below. In addition to the trap drive, colloids are affected by stochastic thermal fluctuations and by the net flow induced by all other moving particles. Experiments are performed increasing the number of beads $N$, maintaining constant the arc-distance between neighboring beads as shown in Fig 2.

### 2.2 Numerical Methods

Brownian Dynamics (BD) simulations, in which the hydrodynamic interaction is calculated through Oseen's tensor[15], are performed to provide a comparison to the experimental data. The algorithm simply solves the equation of motion of the system, with a constant timesteps of $10^{-5}$s. The code has been developed in-house, written in C, and can readily simulate the behavior of systems much larger (e.g. $N \sim 100$) than in the currently possible experiments. The same code was used by ourselves in previous work[10]? . The assumptions for this treatment[16] are a low Re, particles far relative to their diameter, and a steady flow, all of which are satisfied in the physical context.

The "geometric switch" condition is implemented exactly as in the experiment. The "feedback time", i.e. the time interval over which a configuration is tested to actuate the switch in

the position of the potential (which is fixed in the experiments by the acquisition frame rate) can be varied; its effect has been tested previously[10] and is reviewed in the appendix.

### 3 Theoretical background

The steady state dynamics of the geometric switch model can be obtained in principle by solving the dynamic system of equations[17]

$$\mathbf{F}(t)_i - \sum_{j=1}^{n} (\mathbf{H}^{-1})_{i,j} \frac{d\mathbf{r}_j(t)}{dt} + \mathbf{f}_i(t) = 0,$$
$$\mathbf{r}_i(t) \cdot \mathbf{t}(\mathbf{r}_i) = 0, \ i = 1, 2, \cdots, N \quad (1)$$

where the force $\mathbf{F}(t)_i$ acting on the $i^{th}$-particle is harmonic and tangent to the ring, and $\mathbf{t}(\mathbf{r}_i)$ is a versor tangent to the ring, at the position $\mathbf{r}_i$, with anti-clockwise direction. In Eq (1), the second equation imposes that a constraint for each bead to move only along its fixed tangential direction, which is a good approximation for displacements in the physical system due to the active driving of each bead along its tangent direction. The coupling forces scale as $a/d$. As in other work[12,18,19], Eq (1), is describing how the motion of each $j^{th}$-particle originates via the Oseen tensor a force on the $i^{th}$-particle that depends on the whole configuration. The Oseen tensor is given by[16]

$$\gamma H_{ij}^{\alpha\beta} = \delta_{ij}\delta_{\alpha\beta} + (1 - \delta_{ij})\frac{3a}{4r_{ij}}\left(\delta_{\alpha\beta} + \frac{r_{ij}^{\alpha}r_{ij}^{\beta}}{r_{ij}^2}\right),$$
$$\alpha \text{ and } \beta = 1, 2. \quad (2)$$

This can be represented as an $2N \times 2N$ matrix, or equivalently as an $N \times N$ matrix of $2 \times 2$ elements. The distances $r_{ij}$ between
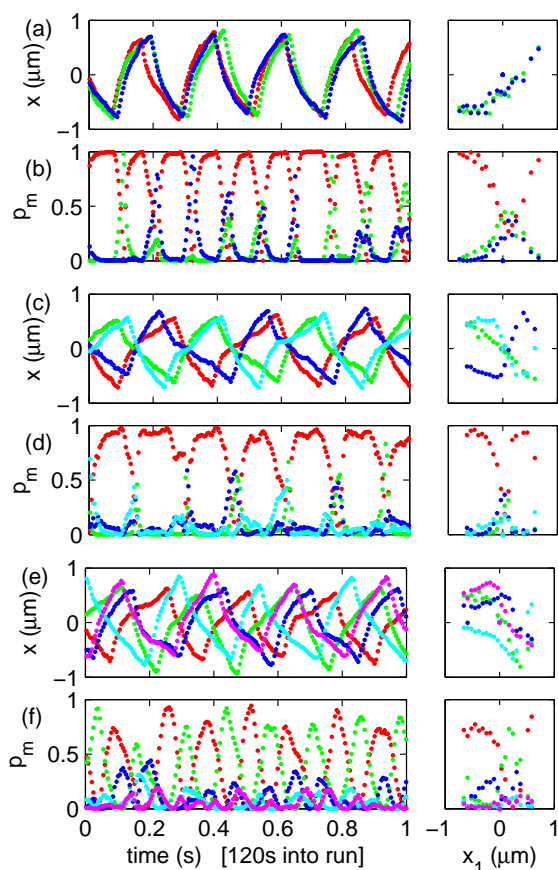
**Fig. 3 Experiments show collective dynamics: the steady state is strongly affected by system geometry.** Shown here are the bead displacements $x(t)$ relative to the mean position, and the projections of the configuration in the steady state onto the hydrodynamic modes of the system. Systems of $N = 3, 4, 5$ are considered, in panels (a,b), (c,d), (e,f) respectively. Large panels show a one-second window of data versus time, whilst the small panels show the mean of the same quantities but plotted versus the position of bead one. The color code red, green, blue, cyan, magenta identifies different beads, anticlockwise. The system dynamics can be globally in-phase for $N = 3$ (a), or nearest neighbors in anti-phase $N = 4$ (c), or a propagating wave for $N = 5$ (e). This is rationalized from the character of the dominant equilibrium modes. In (b), (d), (f) the projections $P_m(t)$, $m = 1, 2, ...N$, onto the eigenvectors of the coupling matrix show an important result: the mode with longest relaxation time (red) dominates the displacement configuration in the non-equilibrium steady state. For $N = 5$, as for larger odd-numbered systems, there are two degenerate modes (red, green), which are seen to alternate in amplitude. The color code indicates decreasing relaxation time: red, green, blue, cyan, magenta. Small panels give the average trajectories over many cycles, plotted as a function of the position of bead-one.
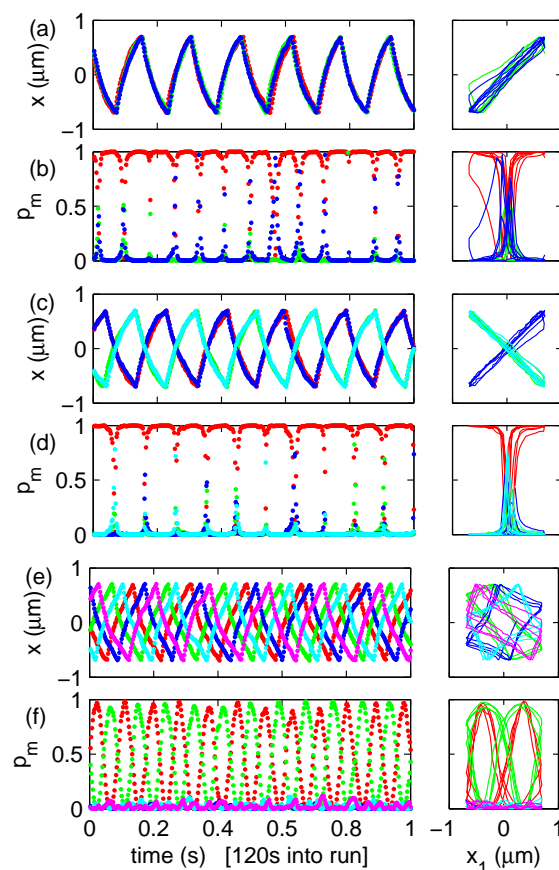
**Fig. 4 Brownian Dynamics simulations with Oseen coupling match the experimental results.** Bead trajectories and projections onto modes for systems of $N = 3, 4, 5$ beads. See the caption of Figure 3 for a description of the colors. These displacements obtained computationally show that the description of hydrodynamic coupling via Oseen's tensor is valid, and confirm that the non-equilibrium dynamics is dominated by the equilibrium normal mode with the longest relaxation time. Small panels give the time average behavior, by plotting bead positions and model projections as a function of the position of bead-one.

the $i^{th}$- and $j^{th}$-particle are in principle time dependent, but can be approximated by their mean values provided that the driving amplitude $A$ is small relative to the mean separation, i.e. $A = \lambda - 2\xi \ll d$. This makes the Oseen tensor in this work independent of time, and just a function of the geometric arrangement of active oscillators.

Eq (1) has a fixed structure (the set of $\mathbf{F}_i$ drive towards a fixed set of positions) in between any bead switch, with the geometric switch rule acting on each bead

$$\mathbf{F}(t)_i = -\kappa \left[ x_i(t) \mp \frac{\lambda}{2} \right] \mathbf{t} \left( \frac{2\pi(i-1)}{N} \right), \qquad (3)$$

where $x_i$ is the displacement along the tangent of the $i^{th}$-bead, one of $\pm\frac{4}{2}$ is the coordinate of the active well minimum, see fig.1.

The stochastic force $\mathbf{f}_i(t)$ in Eq. (1) represents the thermal noise on the $i^{th}$-particle, and it can be assumed that $\langle\mathbf{f}_i(t)\rangle = 0$, $\langle\mathbf{f}_i(t_1)\mathbf{f}_j(t_2)\rangle = 2k_BT\,(\mathbf{H}^{-1})_{ij}\,\delta(t_1 - t_2)$[18].

Eq. (1) changes structure at every switch, making its solution difficult. In a recent paper[17] we have shown how to build analytical solutions in the absence of noise, for symmetric configurations like the ones explored here. The results of the present work show that remarkably the main properties of the steady state solutions can be predicted quite simply from the equilibrium coupling tensor, and hence how they depend on $N$ and the geometry. In the discussion section we outline why this is the case.

## 4 Results

Figure 3 shows the particle positions versus time, for a 1 second interval at steady state during an experiment (data is shown after 120 s have elapsed from the beginning of the driven motion, much longer than the time required to settle into the steady state, which is a few cycles). Movies showing the entire run of these experiments are available as Supplementary Material. Figure 3(a) shows that for $N = 3$ the three beads move in phase with each other, in contrast to $N = 4$ (Fig. 3(c)) where the nearest neighbors are in anti-phase. The behavior of $N = 5$ (Fig. 3(e)) is an apparently more complex synchronized state. We return to this in the discussion section.

Figure 4 shows results of Brownian Dynamics simulations, run for conditions matching the experiments of Figure 3. The BD numerical results have slightly different period in the steady state compared to the experiments, this is simply a difference in the trap stiffness. Performing BD simulations in parallel to experiments has been valuable in this work for two reasons: (1) it is possible to access experimentally challenging conditions (e.g. large $N$), and to isolate the effect of Brownian noise; (2) There are potentially a large number of factors (outlined in the Appendix) that make the experiments potentially more complicated than the simple picture of identical harmonic traps we develop as our model.

It is important to see that the experimental results are very close to the simulations (in which all traps have identical stiffness, perfect harmonicity, etc.). The experiments, in other words, appear to be quite robust to all the potential issues discussed in the Appendix (of which the most important is the resolution of bead position), although some occasional glitches can be observed in the Supplementary Material movies.

In the presence of increasing thermal noise, the bead trajectories and mode amplitudes deviate increasingly from the solutions of the deterministic system, but the solutions remain
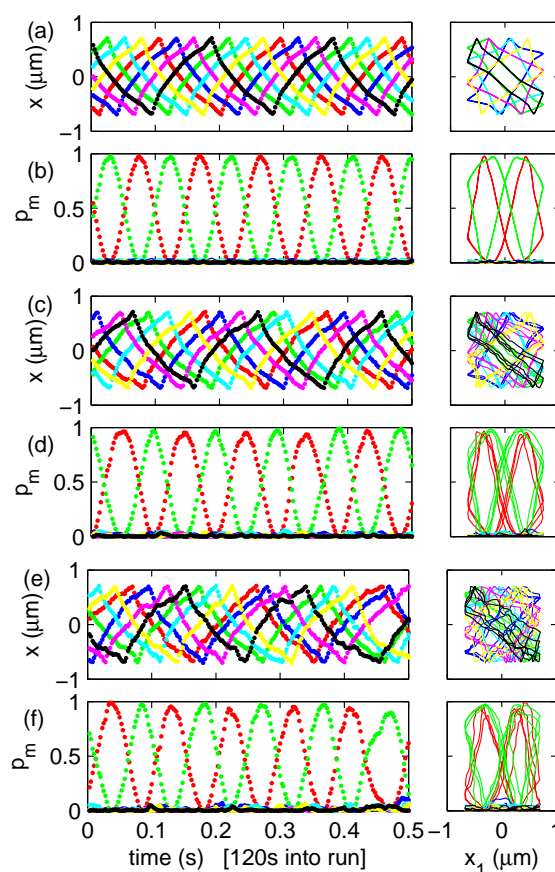


**Fig. 5 The 7-particle system has a traveling wave dynamic state, which is robust to the presence of Brownian noise.** In numerical simulation it is straightforward to tune the level of noise, and it is seen that reducing noise the behavior of the system converges to the deterministic analytical solution. Here, the trajectories and the mode projections of a system of 7 particles are shown for different amplitude of noise, corresponding to temperatures of $T$ =1K (a,b), 273K (c,d) and 1000K (e,f), plotted versus time and versus position of bead one. Other physical parameters are set to the experimental values, and $\kappa$=2 pN/$\mu$m, $\xi = 0.3\,\mu$m. Colors match those in Figures 3, plus yellow and black used for beads (and modes) 6 and 7 respectively. As in previous figures the small panels give the average behavior, plotted as a function of the position of bead-one. The balance of noise relative to hydrodynamic coupling forces can be tuned by changing the physical parameters of the system, as discussed in the text.

stable. This is illustrated in Fig. 5, with numerical data for the system with $N = 7$, in which like $N = 5$ (Figs. 3(f) and 4(f)) and all other odd $N > 3$, there is a degenerate fundamental mode[17], and the dynamic state shows an alternating amplitude of the projections onto these two modes. The trajectories display a fixed phase relation between beads: The nearest neigh-

bors are almost in anti-phase, but delayed by the small interval $T_N/N$. Next-nearest neighbors are almost in-phase, with a delay $2T_N/N$, and so on, describing a propagating wave.

Depending on the initial conditions, at low noise the system will fall into a state where intervals are either positive or negative going around the ring. At higher noise (i.e. higher temperature, or weaker coupling), whilst the system remains overall synchronized, the propagating character is lost over long times because the system is able to flip between the two equivalent states. The large variations in noise levels considered in Fig. 5 cannot of course be achieved experimentally by changing the temperature, since the very high and very low values that are required would affect the physical properties of the media; instead since the hydrodynamic coupling is proportional to $\kappa A^2$ and decays as $(a/d)$, it is possible to tune its importance relative to thermal $k_B T$ by changing the other parameters: $\kappa$, $A$, $a$ and $d$. The loss of synchronization due to noise was explored for the case of two beads in our previous work[10].

# 5 Discussion

The key result of this work is that main features of the complex steady state of the non-linear dynamical system can be predicted from the equilibrium coupling tensor. Underpinning this result is the fact that in-between any two switches, the system of eq. 1 can be linearized for small displacements, and its dynamics is dominated by the slowest Oseen normal mode.

For polygonal arrangements, and neglecting noise, the Oseen coupling matrix is particularly simple: it is the sum of identity and a real symmetric circulant matrix, hence its eigenvalues $m$ and the eigenvectors $\vec{e}^{(m)}$ can be obtained readily[17]. These eigenvectors are the normal modes of the coupled system, and a superposition of them describes the motion in-between switch events.

It is revealing to decompose the configuration at each time $\vec{x}(t)$ onto these normal modes; we consider here the power in each mode $m$, given by $P_m(t) = |\vec{x}(t) \cdot \vec{e}^{(m)}|^2$, and look at its time dependence. In between switch events, each $P_m$ decays exponentially; at each switch, all the $P_m$ are excited, and the non-linear switching periodically precipitates the system in a different state. Experimentally it is clear that for $N = 3$ and $N = 4$ there is a single mode which has very high amplitude (Fig 3(b,d)). In contrast, for $N = 5$ two modes have high amplitude, and they alternate periodically (Fig 3(f)). This behavior is fully confirmed by BD simulations performed as in ref[10], where the Oseen interaction is assumed, see figure 4.

For every *even* value of $N$, the tangential anti-phase motion of pairs of adjacent spheres is the eigenmode with highest drag, and therefore longest relaxation time. For *odd N* clearly it is not possible for all the neighbors to oscillate in anti-phase. With $N > 3$, the eigenmode with the longest relaxation time is degenerate: there are two equivalent modes, in which the

motion of neighbors is almost in anti-phase, but on cycling around the ring each particle is time-shifted by $+\Delta T$ (or $-\Delta T$ in the equivalent mode) relative to its neighbor[17]. The case $N = 3$ is unique, in that the longest relaxation mode is one with all the beads moving in phase. The remarkable result of this study, shown in Fig 3, is that for all $N$ the mode with the highest amplitude is consistently the one with longest relaxation time.

We recall that a system of $N$ beads held in static traps in two dimensions has $2N$ normal modes[12,18–20], and these can be calculated analytically for configurations with high symmetry[12,18]. The constraint for each bead to move only along its fixed tangential direction reduces the number of modes by half, so that there are $N$ normal modes for a $N$ bead system here.

Why is the steady state dynamics largely captured by a normal-mode analysis, and how does the longest lived mode determine the steady state dynamics? The modes described above are a key step in constructing the solutions of the dynamical system: The solutions (for the deterministic, absence of noise, system) are given for each stretch between consecutive switches by linear superposition of the eigenmodes; at each switch, driving potentials change in the system of equations 1,3, and new mode amplitudes are propagated; the condition of periodicity leads to a finite set of solutions[17]. The general feature is that the faster the mode, the more its amplitude has decayed before the following geometric switch. In other words, it is the amplitude of the longest lived mode that "dominates" at the geometric switch, and thus enforces the overall character of the steady state solution.

It is an open question whether this fact is completely generic or it applies only to a range of parameter values. In line of principle, it is possible that the time between two switches is too short for the slowest mode to fully dominate. However, we have not observed this in any of the systems analyzed here.

# 6 Conclusion

Our experimental results highlight the importance of geometry in determining the leading properties of the collective steady state in a driven system. It is remarkable that in this system the equilibrium properties are sufficient to describe the main features of the non-equilibrium emergent dynamics. One may envision that in biological systems, which present complex and often disordered arrangements, and a vast number of oscillators, the behavior highlighted by these simple arrays could represent the local dynamics in tightly coupled sub-systems whose dynamics is simple. In this perspective, the small-system patterns of behavior can be thought of as "dynamical motifs", linked to the geometrical arrangement of beating elements, and that can be analyzed to infer the properties of the individual oscillators.

## Appendix: Experimental Aspects

The experiments (contrast the experiments of Figure 3 to its numerical counterpart Figure 4) share the character of the steady state, which is the key observation of this work, but are somewhat "noisier" than the simulations. We outline here possible reasons for this.

### The switch-position resolution

The particle positions are obtained in real time at the frame rate of the acquisition (between 200 and 300 Hz, depending on the image size). The calculation is carried out in the computer, by standard methods: A correlation filtering (with an optimised mask profile) is followed by sub-pixel interpolation of the maximum in the filtered image. In principle, as shown by the Grier group, the resolution of the detection by these methods can be as good as a few 10 nm. In practice, with the high frame rate camera and real-time operation, we have determined that experimentally the standard deviation of the switch positions of a driven bead is 74 nm. This value is the significant quantity in our experiment, and its scatter is dominated by the imaging resolution. We know this because running the Brownian Dynamics simulation, under identical feedback time and other parameters to the experiment, we obtain a standard deviation of the switch positions of 7.5nm. This latter, simulated value, includes the effects of Brownian noise, and of the finite feedback time, but in contrast to the experiment it does not include any error in position resolution or in the time to communicate a switch into the laser trap positions (the simulation has no such errors).

So particle position resolution is the main source of uncertainty in the experiments, and we think it is the reason for the increased "noise" compared to simulations with matching parameters.

### The switch-timing resolution

The position detection calculation, written in c++ and carried out on a fast workstation on each frame, is not the rate-limiting step. The rate-limiting step in our current feedback system is that as a result of this position determination, the computer sends a command to the electronics that controls the AOD laser deflection. The timing of this command is under the control of the operating system: We use a server-grade computer with multiple multicore processors, running Linux with the RT PREEMPT patch to approach real-time scheduling by the operating system. There remains some timing uncertainty which is beyond our control. To summarise on timing: an image arrives into the computer RAM from the CMOS camera, it is analysed, and a control command sent to the electronics, before the next image arrives.

The total feedback time can in principle be important. The influence of feedback time was studied extensively in the 2-bead case in previous work, ref[10], and we had found that provided the feedback loop was accomplished in a small fraction of the relaxation times, it had no effect on the steady state. Here in this work we also checked its effect by changing feedback time (i.e. the time interval at which the system is interrogated to determine if there is to be a switch in the potentials) in the Brownian Dynamics simulations. Like in the previous work, in the experimentally relevant range of feedback time (which is a small fraction of all the relevant timescales in the system), there is no effect on the character of the stable solution.

### Harmonicity and homogeneity of the traps

Optical tweezer potentials are only imperfect harmonic wells: (a) even in optimally aligned systems, the linear polarisation of the laser confers some directional anisotropy; (b) traps across the field of view may not have exactly the same stiffness; (c) at large displacements, they stop being harmonic; (d) colloidal particles have themselves a small polydispersity, and this correlates with how stiffly each is trapped. We do not think that these factors play a major role in the current experiment, and the excellent qualitative agreement with simulations in which none of these aspects is present supports this.

## References

1 M. Polin, I. Tuval, K. Drescher, J. Gollub and R. Goldstein, *Science*, 2009, **325**, 487 – 490.

2 J. J. Breunig, J. I. Arellano and P. Rakic, *Nature Neuroscience*, 2010, **13**, 654–655.

3 A. S. Kozlov, J. Baumgart, T. Risler, C. P. C. Versteegh and A. J. Hudspeth, *Nature*, 2011, **474**, 376–379.

4 S. Gueron, K. Levit-Gurevich, N. Liron and J. Blum, *Proc. Natl. Acad. Sci.*, 1997, **94**, 6001–6006.

5 R. Golestanian, J. Yeomans and N. Uchida, *Soft Matter*, 2011, **7**, 3074.

6 E. Lauga and T. R. Powers, *Rep. Prog. Phys.*, 2009, **72**, 096601.

7 T. Niedermayer, B. Eckhardt and P. Lenz, *Chaos*, 2008, **18**, 037128.

8 N. Uchida and R. Golestanian, *Phys. Rev. Lett.*, 2011, **106**, 058104.

9 M. Cosentino Lagomarsino, P. Jona and B. Bassetti, *Phys. Rev. E*, 2003, **68**, 021908.

10 J. Kotar, M. Leoni, B. Bassetti, M. Cosentino Lagomarsino and P. Cicuta, *Proc. Natl. Acad. Sci.*, 2010, **107**, 7669–7673.

11 C. Wollin and H. Stark, *Eur. Phys. J. E*, 2011, **34**, 42.

12 G. M. Cicuta, J. Kotar, A. T. Brown, J. Noh and P. Cicuta, *Phys. Rev. E*, 2010, **81**, 051403.

13 M. Leoni, J. Kotar, B. Bassetti, P. Cicuta and M. Cosentino Lagomarsino, *Soft Matter*, 2009, **5**, 472 – 476.

14 R. C. Weast and M. J. Astle, *CRC Handbook of Chemistry and Physics, 60th Ed.*, CRC Press, Boca Raton, 1979.

15  D. L. Ermak and J. A. McCammon, *J. Chem. Phys.*, 1978, **69**, 1352–1360.

16  J. Happel and H. Brenner, *Low Reynolds Number Hydrodynamics: with special applications to particulate media*, Kluwer, New York, 1983.

17  G. M. Cicuta, E. Onofri, M. Cosentino Lagomarsino and P. Cicuta, *Phys. Rev. E*, 2012, **85**, 016203.

18  M. Polin, D. Grier and S. Quake, *Phys. Rev. Lett.*, 2006, **96**, 088101.

19  R. Di Leonardo, S. Keen, R. Leach, C. D. Saunter, G. D. Love, G. Ruocco and M. J. Padgett, *Phys. Rev. E*, 2007, **76**, 061402.

20  J. C. Meiners and S. R. Quake, *Phys. Rev. Lett.*, 1999, **82**, 2211–2214.